

A (hetero)arylidene-(4-substituted-thiazol-2-yl) hydrazine As New Potential MAO-B inhibitors. Computational Study and In-Silico Prediction

Moulay Ahfid El ALAOUY*, Marwa ALAQARBEH**, Abdelouahid SBAI***, Hamid MAGHAT****, Tahar LAKHLIFI****, Mohammed BOUACHRINE*****

A (hetero)arylidene-(4-substituted-thiazol-2-yl) hydrazine As New Potential MAO-B inhibitors. Computational Study and In-Silico Prediction

SUMMARY

The inhibitory effect of 44 hydrazine derivatives (4-substituted-thiazole-2-yl) compounds against hMAO-B was evaluated to understand the structure-activity-relationship. The results show that the CoMFA/SE model has high stability and predictability ($Q_2 = 0.608$; $R_2 = 0.933$; $R_2 \text{ Test} = 0.70$). Contour maps derived from the CoMFA/SE vacuum field and the electrostatic field provide more information about the modulation of these inhibitors.

The interactions were investigated by molecular docking and showed a conventional hydrogen bond with residues Ile14, Ser15, Gln206, Met436, Tyr435, Tyr60, and Ser59, which play essential roles in the biological field. The MD binding free energies for compound 26 and proposed compound M1 with hMAO-B of -134.288 kJ/mol and -150.506 kJ/mol , respectively, were -134.288 kJ/mol and -150.506 kJ/mol , respectively. Therefore, compound M1 is more active than compound 26 at the active site of the hMAO-B receptor.

Key Words: ADMET, 3D-QSAR, Molecular Docking, Molecular Dynamics, hMAO-B.

Yeni Bir Potansiyel MAO-B İnhibitörü Olarak Bir (hetero) ariliden-(4-süstitüe-tiyazol-2-il) hidrazin. Hesaplamalı Çalışma and in-Silico Tabmin

ÖZ

Yapı-aktivite-ilişkisini anlamak amacıyla 44 hidrazin türevi (4-süstitüe-tiyazol-2-il) bileşiğin hMAO-B'ye karşı inhibitör etkisi değerlendirilmiştir. Sonuçlar CoMFA/SE modelinin yüksek kararlılığa ve tahmin edilebilirliğe sahip olduğunu göstermektedir ($Q_2 = 0.608$; $R_2 = 0.933$; $R_2 \text{ Test} = 0.70$). CoMFA/SE vakum alanı and elektrostatik alandan elde edilen sınır haritaları, bu inhibitörlerin modülasyonu hakkında daha fazla bilgi sağlar.

Etkileşimler moleküler yerleştirme yöntemi ile incelenmiş and biyolojik alanda önemli roller oynayan Ile14, Ser15, Gln206, Met436, Tyr435, Tyr60 and Ser59 kalıntılarıyla geleneksel bir hidrojen bağının varlığı gösterilmiştir. Bileşik 26 and önerilen bileşik M1'in hMAO-B ile MD bağlanma serbest enerjileri sırasıyla -134.288 kJ/mol and -150.506 kJ/mol 'dür. Bu nedenle, M1 bileşiği hMAO-B reseptörünün aktif bölgesinde bileşik 26'dan daha aktiftir.

Anahtar Kelimeler: ADMET, 3D-QSAR, Moleküler Yerleştirme, Moleküler Dinamik, hMAO-B

Received: 1.04.2024

Revised: 29.09.2024

Accepted: 10.10.2024

* ORCID: 0009-0005-1593-1486 Molecular Chemistry and Natural Substances Laboratory, Faculty of Science, University Moulay Ismail, Meknes, Morocco

** ORCID: 0000-0002-0879-5077 Basic Science Department, Prince Al Hussein bin Abdullah II Academy for Civil Protection, Al-Balqa Applied University, Al-Salt 19117, Jordan

*** ORCID: 0000-0002-7140-9853 Molecular Chemistry and Natural Substances Laboratory, Faculty of Science, University Moulay Ismail, Meknes, Morocco

**** ORCID: 0000-0002-7731-330X Molecular Chemistry and Natural Substances Laboratory, Faculty of Science, University Moulay Ismail, Meknes, Morocco

***** ORCID: 0000-0003-4917-475X Molecular Chemistry and Natural Substances Laboratory, Faculty of Science, University Moulay Ismail, Meknes, Morocco

***** ORCID: 0000-0002-8901-047X Molecular Chemistry and Natural Substances Laboratory, Faculty of Science, University Moulay Ismail, Meknes, Morocco

INTRODUCTION

Monoamine oxidase (MAO) is an oxidoreductase enzyme that catalyze monoamine neurotransmitters, and they belong to flavin adenine dinucleotide (FAD)-dependent protein (Yang et al., 2017). The deamination of neurotransmitters and biogenic amines is catalyzed by the flavoproteins MAO (Yücel and Özdemir, 2023), which has two distinct isoforms, A and B (MAO A and MAO B) (Chimenti et al., 2007). MAO-A metabolizes the ample endogenous amine serotonin, while MAO-B metabolizes small amines such as phenylethylamine, the precursor of dopamine and norepinephrine, a precursor to dopamine and norepinephrine. As a result, human MAO inhibitors (hMAO-Is) play a significant role in managing neurological and psychiatric illnesses. In particular, hMAO-A inhibitors are employed as antidepressants and anxiolytics, whereas hMAO-B inhibitors are adjuncts in treating PD (Secci et al., 2012a). MAO-B kinetics gets stronger with age in the brain, along with the increase of the catalytic process of oxidative deamination, which produces aldehydes and hydrogen peroxide as by-products (Lu et al., 2018) nanostructured NS. Since oxidative stress and the development of neuronal damage are linked, inhibition of MAO-B will likely prevent the brain from metabolizing monoamines, thereby counteracting the degenerative consequences (Vicente-Zurdo et al., 2023). The hMAO-B inhibitors are helpful and successful in reducing motor fluctuations in people with early and advanced Parkinson's disease (PD) by improving dopamine levels and reducing the side effects of PD treatments (Kondeva-Burdina et al., 2022a). In this regard, using specific hMAO-B inhibitors to treat PD is warranted because oxidative deamination of the primary monoamine by hMAO produces toxic NH_3 , aldehyde, and H_2O_2 agents (Dhiman, Malik, Sobarzo-Sánchez, Uriarte and Khatkar, 2019). Because of the increase in hMAO activity and the consequent increase in H_2O_2 production by hMAO-B, age-related degenerative

disease processes, Parkinson's may also be related to oxidative stress. Therefore, inhibitors of hMAO-B could work by reducing free radical production and increasing monoamine levels in the brain (Kondeva-Burdina et al., 2022b). In treating PD, MAO-B inhibitors play a crucial role in preserving dopamine levels in the brain and alleviating the symptoms of the disease (Bozbey, Taşkor Önel, Türkmenoğlu, Gürsoy and Dilek, 2022). Several heterocyclic compounds have been studied to investigate the potential MAO-B enzyme inhibition activity. 4-substituted thiazol-2-yl hydrazines belong to thiazole heterocyclic derivative and have been shown to bind to MAO-B enzyme and block its activity, thus helping preserve dopamine levels (Anastassova et al., 2022; Chimenti et al., 2010). Also, benzimidazoles and isoquinolines, other heterocyclic compounds, have interesting therapeutic targets for treating Parkinson's disease (Anastassova et al., 2022; Nagatsu, 1997). Further research has examined MAO-B inhibitors such as selegiline and rasagiline for their neuroprotective effects in PD by preserving dopamine levels (Fiddian-Green and Silen, 1975). Discovering and designing new MAO-B inhibitors as potential drugs to treat Parkinson's disease using computer-aided methods such as three-dimensional quantitative structure-activity relationship (3D-QSAR), molecular docking, ADMET predictions, and molecular dynamics (MD) simulations have been used to design potential candidate drugs (Aanouz et al., 2021). In this work, comparative molecular domain analysis (CoMFA) was performed on 44 hydrazine (4-substituted-thiazole-2-yl) derivatives synthesised by Daniela Secci et al. to relate the characteristic structure to the inhibitory activity of the hMAO-B enzyme (Secci et al., 2012). Molecular docking and ADMET studies facilitate the identification of new drug candidates. Finally, molecular dynamics simulation at 100 ns was performed to estimate the binding stability of 44 candidates within the target protein to confirm the docking results.

MATERIALS AND METHODS

Data collection

This study investigated 44 (hetero)arylidene-(4-substituted-thiazol-2-yl) hydrazine derivatives synthesised by Secci et al. were investigated as potential selective inhibitors of human MAO-B inhibitors. (Secci et al., 2012). The inhibitory activities of compounds IC_{50} (M) values were changed to a logarithmic scale ($pIC_{50} = -\log IC_{50}$), as shown in (Table 1) and (Figure 1.). 35 compounds were used

as a training set, and the remaining 9 inhibitors were used to validate the developed model. 3D-QSAR modeling was performed using Sybyl software, and the Gasteiger-Huckel method was used to add the partial atomic charges after the Tribe force field lowered the resulting energy. The convergence value of the Powell gradient energy was set to 0.005 kcal/mol A, and the maximum number of iterations was 1000 to produce an efficient 3D-QSAR model (Fiddian-Green and Silen, 1975).

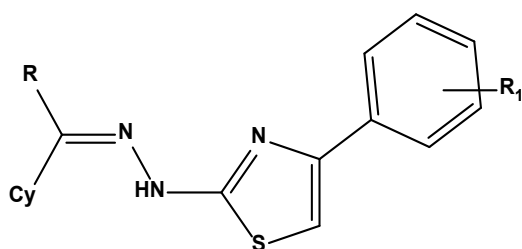
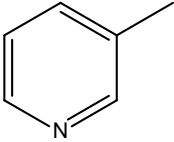
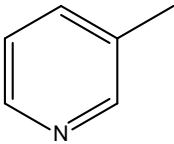
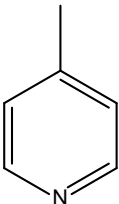
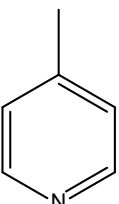
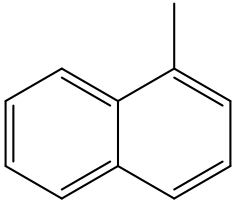
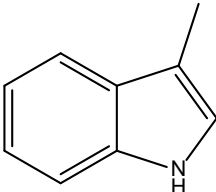
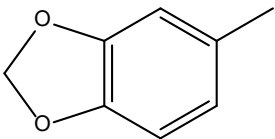
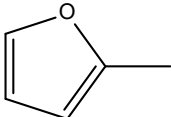
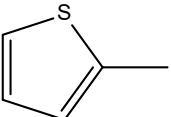
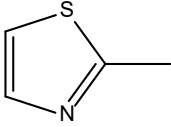
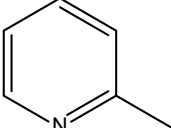
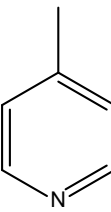
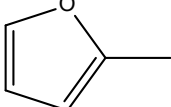
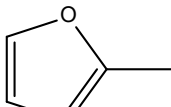
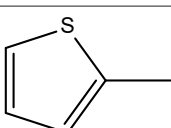
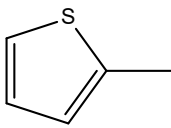
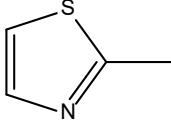
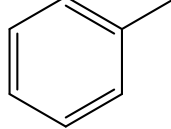
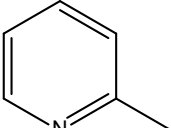
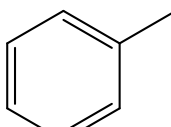


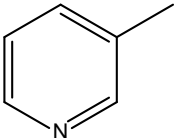
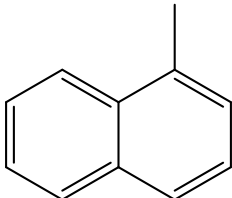
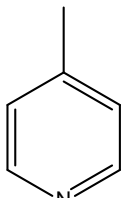
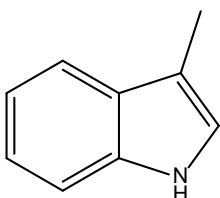
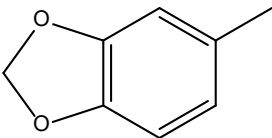
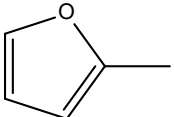
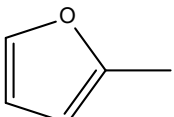
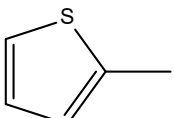
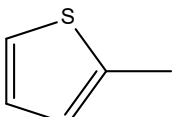
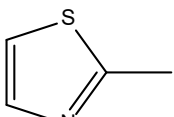
Figure 1. The chemical formula of the studied compounds.

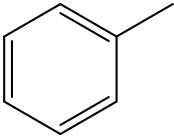
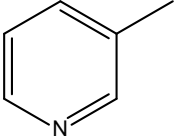
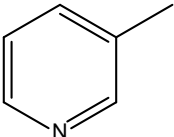
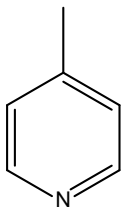
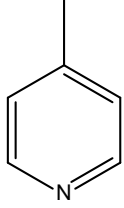
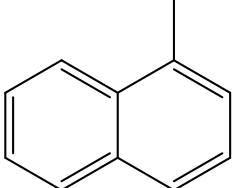
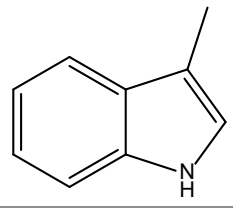
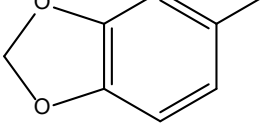
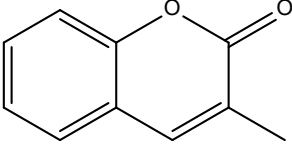
Table 1. Activities and structures of (hetero) arylidene-(4-substituted-thiazol-2-yl) derivatives.

No	Cy	R	R1	IC_{50} hMAO-B	pIC_{50} hMAO-B
1		H	4-CN	1.49 μ M	5.827
2		H	4-CN	152.86nM	6.815
3*		CH ₃	4-CN	3.11 μ M	5.507
4		CH ₃	4-CN	2.00 μ M	8.699
5		CH ₃	4-CN	995.94 nM	6.001

6		H	4-CN	946.62 nM	6.023
7		CH ₃	4-CN	2.09 nM	8.68
8		H	4-CN	6.75 μM	5.17
9*		CH ₃	4-CN	435.91 nM	6.36
10		H	4-CN	1.10 μM	5.958
11		H	4-CN	762.37nM	6.118
12		H	4-CN	301.10 nM	6.521
13		CH ₃	4-NO ₂	3.59 μM	5.445
14		CH ₃	4-NO ₂	297.91 nM	6.526

15		CH ₃	4-NO ₂	366.21 nM	6.436
16*		CH ₃	4-NO ₂	26.67 nM	7.574
17*		CH ₃	4-NO ₂	13.12 nM	7.882
18		H	4-F	652.80 nM	6.185
19		CH ₃	4-F	319.82 nM	6.495
20		H	4-F	338.35 nM	6.47
21		CH ₃	4-F	15.49 nM	7.81
22*		CH ₃	4-F	1.21 μM	5.917
23		CH ₃	4-F	350.70 nM	6.455
24*		CH ₃	4-F	24.31 nM	7.614
25		H	4-F	482.16 nM	6.316

26		CH ₃	4-F	1.70 nM	8.769
27*		H	4-F	12.82 μM	4.892
28		H	4-F	112.36 nM	6.95
29		H	4-F	577.99 nM	6.238
30		H	4-F	1.08 μM	5.966
31*		H	2,4-F	216.58 nM	6.664
32		CH ₃	2,4-F	40.08 nM	7.397
33		H	2,4-F	16.58 nM	7.78
34		CH ₃	2,4-F	3.01 nM	8.521
35		CH ₃	2,4-F	12.96 nM	7.887

36		CH ₃	2,4-F	90.26 nM	7.044
37 *		H	2,4-F	198.50 nM	6.702
38		CH ₃	2,4-F	18.40 nM	7.735
39		H	2,4-F	548.85 nM	6.26
40		CH ₃	2,4-F	16.68 nM	7.777
41		H	2,4-F	137.6 nM	6.861
42		H	2,4-F	529.48 nM	6.276
43		H	2,4-F	1.17 μM	5.931
44		CH ₃	2,4-F	1.42 μM	5.847

* Test set

Alignment of the inhibitors

One of the most critical aspects of the structural alignment of target compounds significantly impacts the predictive ability and accuracy of 3D QSAR models and the reliability of contour maps. In this paper, the least energetic conformation of the most

active compound 26 has been considered as the superposition model (Stamm, Latscha, Janecek and Campana, 1976). The other inhibitors were aligned with the common backbone, and the alignment results are shown in (Figure 2).

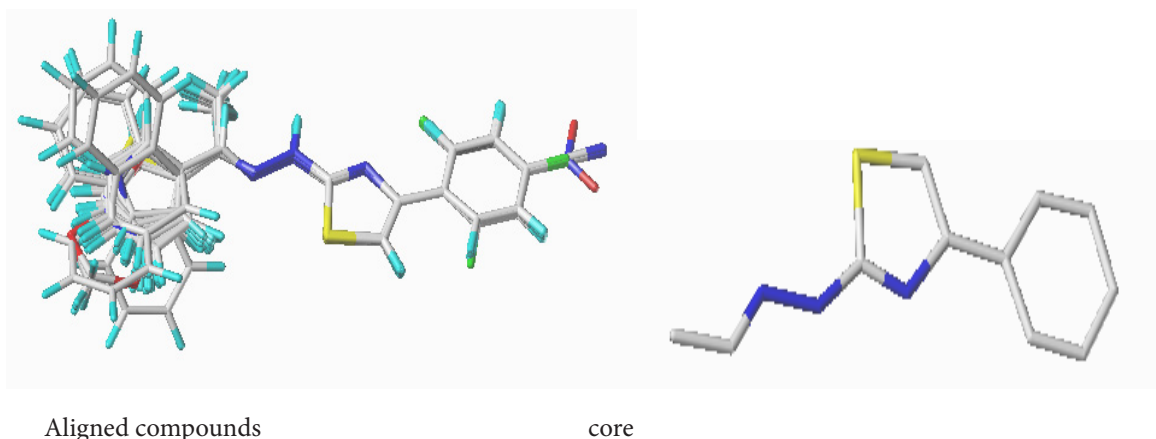


Figure 2. Overlay and alignment of the 44 molecules using Molecule 26 as a model.

Generation of 3 D-QSAR models

CoMFA and CoMSIA are three-dimensional quantitative structure-activity relationship (3D-QSAR) methods used to describe the properties of receptor interactions and chemical bonds. Carbon sp³ with a charge of +1 was used as a probe with a van der Waals radius of 1.52 and default energy cut-off values of over 30 kcal mol⁻¹ to determine field energies. In addition, Gasteiger-Huckel charges were calculated. CoMFA and CoMSIA fields were automatically calculated using the standard Sybyl method for each molecule, using the Tripos force field in a cubic grid in all directions.

Partial least square (PLS) statistical analysis

The PLS approach was employed to construct the CoMFA and CoMSIA models, with the activity of the 35 molecules in the training set used as the dependent variable for pattern matching and the pattern descriptors as the independent variables (Şener, Ekici, Gönülalan and Bodur, 2024). Regression analysis using PLS created accurate and focused models. The sp³ carbon with a charge of +1.0 was used to generate all the required fields. Initially, the cross-validated

determination coefficient q^2 and the optimal number of components (ONC) were determined using a cross-validation analysis approach with a Leave-One-Out (LOO) technique. Subsequently, the model was evaluated using a cross-validated analysis based on the determination coefficient (R^2), the standard error of estimation (SEE), and the F-value (Lipscomb, Scott and Schulman, 2010).

ADMET Prediction

The physicochemical and biological properties of small molecules are essential to determine the utility of drug candidates by integrating Lipinski's rules and ADMET predictions using the Swiss-ADMET web server (Daina, Michielin and Zoete, 2017). This resource is freely available. The six designed molecules (M1-M6) and compound 26 were submitted in silico using the five Lipinski rules (Pires, Blundell and Ascher, 2015) molecular weight (MW) ≤ 500 , $\log p < 5$, hydrogen bond donors (HBD) ≤ 5 , number of hydrogen bond acceptors (HBA) ≤ 10 , and rotational bonds (nrotb) ≤ 10 , and additionally topological polar area (TPSA) ≤ 140 Water solubility, human intestinal absorption, Molar refractoriness should be between

40 and 130, metabolism, Cytochrome P450 enzymes, synthetic accessibility score and toxicity (Boutalaka et al., 2023).

Molecular docking

Prediction of binding patterns of ligands with target proteins has long been achieved through molecular docking method. Many research and commercial tools are currently available for protein docking. This study used a new molecular docking tool called CB-Dock, identifying binding sites, size, and position of protein and target molecules. The appropriate docking size is based on the query links and performs molecular docking using AutoDock (Kahn, Bosch, Levitt and Goldstein, 1975) the increment in Na and Cl reabsorbed beyond the proximal tubule. The administration of these agents resulted in an increase in fractional sodium excretion (CNa/GFR). The server collaborates with AutoDock Vina and has undergone extensive optimization to increase the success rate of the created models. In this study, the researchers used the web server <http://caolabshare.cn/cb-dock/> (Liu et al., 2020). The data entry includes ligand files in MOL2, MOL, or SDF format for compound 26 and the proposed compounds (M1, M2, M3, M4, M5, and M6.), which were selected as new candidates due to their pharmacokinetic properties (Stitou et al., 2021). In addition, the enzyme (hMAO-B) was also downloaded in PDB format from www.rcsb.org (PDB: 2V60) (Shaikat and Hussain, 2022). Crystallized water molecules, heteroatoms, etc., were automatically removed from the protein when uploaded to the CB-Dock web server. After uploading, CB-Dock uses OpenBabel to read the input files and convert them to pdbqt format (Cao and Li, 2014).

Molecular Dynamics Simulations

The CHARMM-GUI solution builder consists of five steps for setting up a simulation system. In the third step, Periodic Boundary Conditions (PBC) are established by replicating a unit cell in all directions to approximate a larger system. The simulation

is then conducted solely for the atoms within the PBC box. Additionally, any unfavorable contacts between atoms are eliminated by performing a short minimization during this step. The fourth and fifth steps involve the equilibration and production phases of the simulation. Equilibration is achieved through two phases: the NVT ensemble (constant number of particles, volume, and temperature) and the NPT ensemble (constant number of particles, pressure, and temperature) (Kahn et al., 1975) the increment in Na and Cl reabsorbed beyond the proximal tubule. The administration of these agents resulted in an increase in fractional sodium excretion (CNa/GFR). These phases ensure that the system reaches the desired temperature and pressure equilibrium. Input files for equilibration and production, along with anticipated modifications such as the molecular dynamics (MD) run duration and the frequency of energy calculations, are downloaded. GROMACS 2020. 2, a software widely used for MD simulations, was employed for both equilibration and production runs in all MD calculations. The simulation setup involved the imposition of PBC considering the shape and size of the system. Non-bonded interactions were handled with a cutoff distance of 12 Å, and the neighbor searching list was buffered using the Verlet cutoff scheme. Long-range electrostatic interactions were treated using the particle mesh Ewald (PME) method. The CHARMM36 force field was applied to the protein-ligand complex. Prior to production simulation, an energy minimization step using the steepest descent algorithm was performed with 5000 steps to reduce the system's energy. To stabilize the complex, an equilibration process was conducted (Pajzderska and Gonzalez, 2023). The complex was subjected to an NVT ensemble and an NPT ensemble for duration of 125 ps at a temperature of 300.15 K. Positional restraints of 400 kJ mol⁻¹ nm⁻² and 40 kJ mol⁻¹ nm⁻² was applied to the backbone and side chains, respectively. Following equilibration, a production simulation was conducted for 100 ns in an NPT ensemble at 300.15 K and 1 bar pressure. A

nose-hoover thermostat was employed to maintain a constant temperature, while a Parrinello-Rahman barostat was used to control the pressure. The LINCS algorithm was utilized to constrain hydrogen bonds based on the inputs provided by CHARMM-GUI. The V-rescale thermostat at 300 K with a coupling constant of 1 ps was employed. Trajectories were stored every 2 ps. The production stage involved performing 100 ns simulations in an NPT assembly (Kidder and Montgomery, 1975).

Binding Energy Calculations

The Poisson-Boltzmann method or the Born MM/PBSA series continuous soluble surfactant is a commonly used and widely accepted method for calculating the binding free energy of a protein-ligand complex. Calculations of the binding free energy and the energy contribution of individual residues were used to estimate the inhibitory affinity of ACHE quantitatively (Fiddian-Green and Silen, 1975). The “g_mmpbsa, a GROMACS tool” was used with default parameters to calculate molecular mechanics potential energy (electrostatic van der Waals interactions) and insoluble energy (non-polar

solubility energies) (Lévêque-Simon et al., 2023).

The binding free energy can be expressed using the following equation:

$$\Delta G_{binding} = \Delta G_{complex} - (\Delta G_{protein} + \Delta G_{ligand})$$

where, $\Delta G_{complex}$ is the total free energy of the protein-ligand complex, and are the total free energies of the isolated protein and ligand in the solvent, respectively (Zwahlen, 2023).

RESULTS AND DISCUSSION

CoMFA analysis

The statistical results of the CoMFA/SE model are listed in (Table 2), where PLS analysis of CoMFA/SE model reveals that 9 was the ideal number of components. Q^2 value was 0.608 (>0.5), the correlation coefficient (R^2) was 0.933, the F value was 38.555, and the standard error (SEE) was 0.307. R^2 test value of 0.70 reflects that molecules in the test set agree with the CoMFA model. Also, it demonstrates the strong predictive ability of the CoMFA/SE model. The contribution of the steric field was 47.4%, which was slightly lower than the contribution of the electrostatic field, which was 52.6%.

Table 2. S E results.

	Q^2	N	SEE	R^2	F	R^2 Test
S + E	0.608	9	0.307	0.933	38.555	0.70

CoMSIA analysis

During the CoMSIA analysis, 9 models were built based on the statistical parameter values. The results of these models, using different combinations of five variables, are presented in (Table 3). Among these models, the combined model (CoMSIA/S+E+A+H) showed the best performance with $Q^2 = 0.53$, $R^2 = 0.88$, $F = 20.463$, $SEE = 0.41$, and $ONC = 4$. The model

was then validated with the test set, producing an R^2 test value of 0.79, indicating its effectiveness and predictive ability compared to other models. Notably, the CoMFA (S+E) model presented higher Q^2 and R^2 values than the (CoMSIA/S+E+A+H) model, making it the most appropriate choice to provide better statistical information in this research (El Bahi, Boutalaka, El Alaouy, et al., 2023).

Table 3. Possibilities of combining (COMSIA) fields.

	Q ²	N	SEE	R ²	F	R ² Test
H	0.527	9	0.417	0.87	19.64	0.673
S+H	0.53	9	0.412	0.879	20.18	0.77
S+E+A+H	0.53	4	0.41	0.88	20.463	0.79
S+E+D+A+H	0.516	5	0.408	0.881	20.637	0.79
D+A+E+H	0.52	5	0.414	0.878	20.028	0.78
S+D+H	0.463	9	0.439	0.863	17.49	
E+H+S	0.45	7	0.43	0.868	18.28	0.47
H+D	0.40	9	0.426	0.871	18.72	0.53
E+H	0.48	7	0.434	0.866	17.941	0.44

The actual and predicted activity results of the CoMFA/S+E and COMSIA/S+E+A+H models for hMAO-B inhibitors are presented in (Table 4).

Table 4. Experimental and predicted pIC₅₀ of the CoMFA/S+E and COMSIA/S+E+A+H models

N	pIC ₅₀ (M)	(CoMFA/SE)/(Predicted	residuals)	(COMSIA/SEAH)/(Predicted	Residuals)
1	5.827	5.942	-0.115	5.861	-0.034
2	6.815	7.011	-0.196	7.021	-0.206
3*	5.507	8.274	-2.767	8.079	-2.572
4	8.699	8.602	0.097	8.165	0.534
5	6.001	6.028	-0.027	6.036	-0.035
6	6.023	6.18	-0.157	6.316	-0.293
7	8.68	8.287	0.393	8.215	0.465
8	5.17	5.302	-0.132	5.689	-0.519
9*	6.36	7.059	-0.699	7.401	-1.041
10	5.958	5.849	0.109	5.935	0.023
11	6.117	6.192	-0.075	6.149	-0.032
12	6.521	6.468	0.053	6.455	0.066
13	5.445	5.541	-0.096	5.424	0.021
14	6.526	6.692	-0.166	6.5	0.026
15	6.436	6.32	0.116	6.418	0.018
16*	7.574	5.928	1.646	6.38	1.194
17*	7.882	5.807	2.075	5.162	2.72
18	6.185	6.076	0.109	5.704	0.481
19	6.495	6.356	0.139	6.871	-0.376
20	6.47	6.517	-0.047	6.725	-0.255
21	7.81	7.712	0.098	7.995	-0.185
22*	5.917	7.734	-1.817	7.698	-1.781
23	6.455	6.601	-0.146	6.335	0.12
24*	7.614	5.615	1.999	5.625	1.989
25	6.316	5.993	0.323	6.045	0.271
26	8.769	8.413	0.356	8.16	0.609
27*	6.949	4.867	2.082	5.344	1.605
28	4.892	5.328	-0.436	5.601	-0.709
29	6.238	6.324	-0.086	6.17	0.068
30	5.966	5.865	0.101	6.112	-0.146
31*	6.664	7.196	-0.532	6.865	-0.201
32	7.397	7.433	-0.036	7.52	-0.123
33	7.78	7.446	0.334	7.312	0.468
34	8.521	8.315	0.206	8.515	0.006
35	7.887	8.126	-0.239	8.53	-0.643
36	7.044	7.047	-0.003	6.928	0.116
37*	6.702	6.803	-0.101	6.526	0.176
38	7.735	8.782	-1.047	8.497	-0.762
39	6.26	6.102	0.158	5.981	0.279
40	7.777	7.701	0.076	7.698	0.079
41	6.861	6.435	0.426	6.194	0.667
42	6.276	6.34	-0.064	6.08	0.196
43	5.931	5.924	0.007	6.008	-0.077
44	5.847	5.879	-0.032	5.966	-0.119

* Test set

External validation

In order to assess the predictive capacity of the best CoMFA models developed, external validation was

carried out on nine compounds. These compounds were randomly selected and excluded from the initial study.

Table 5. The results of tests carried out by Golbraikh and Tropsha

Parameter	Equation	COMFA	COMSIA	Validation Criteria
R ² (test)	$R_{test}^2 = 1 - \frac{\sum (Y_{pred(test)} - Y_{obs(test)})^2}{\sum (Y_{obs(test)} - \bar{Y}_{obs(test)})^2}$	0.70	0.79	>0.60
r ₀ ²	$r_0^2 = 1 - \frac{\sum (Y_{obs(pred)} - kY_{test(pred)})^2}{\sum (Y_{test(pred)} - \bar{Y}_{test(pred)})^2}$	0.997	0.999	>0.50
r' ₀ ²	$r_0'^2 = 1 - \frac{\sum (Y_{test} - kY_{test})^2}{\sum (Y_{test} - \bar{Y}_{test})^2}$	0.736	0.703	>0.50
Δr ₀ ²	r ₀ ² - r' ₀ ²	0.260	0.296	< 0.30
$\frac{(r^2 - r_0^2)}{r^2}$	$\frac{(r^2 - r_0^2)}{r^2}$	-0.428	-0.257	< 0.10
$\frac{(r^2 - r_0'^2)}{r^2}$	$\frac{(r^2 - r_0'^2)}{r^2}$	-0.0547	0.115	< 0.10
K	$k = \frac{\sum (Y_{obs} \times Y_{pred})^2}{\sum (Y_{pred})^2}$	0.991	0.997	0.85 ≤ K ≤ 1.15
K'	$k' = \frac{\sum (Y_{obs} \times Y_{pred})^2}{\sum (Y_{obs})^2}$	0.943	0.939	0.85 ≤ K' ≤ 1.15

The statistical results show that the CoMFA and CoMSIA/SEHA models have a good predictive quality, corroborated by the coefficients of determination obtained in the non-cross-validation and cross-validation and the predictive ability demonstrated in the external validation. The robustness of the proposed model was assessed using Tropsha and Golbraikh's external validation criteria. The results obtained in the external validation test for the CoMFA and CoMSIA/

SEHA models are presented in (Table 5).

Y-randomization test of model

The quality of the QSAR model was tested by running ten tests with randomized methods, as shown in (Table 6). The results of the Y randomization test showed lower Q² and R² values than the model in the current study, indicating that the CoMFA/SE model was not obtained in a systematically randomized manner.

Table 6. R²_{train} and Q² LOO values after the Y-randomization experiments.

Model	R	R ²	Q ²
Random 1	0.137	0.018	-0.102
Random 2	0.202	0.041	-0.106
Random 3	0.259	0.067	-0.039
Random 4	0.048	0.002	-0.095
Random 5	0.245	0.06	-0.05
Random 6	0.022	0.0004	-0.128
Random 7	0.07	0.005	-0.15
Random 8	0.0013	0.000	-0.085
Random 9	0.025	0.0006	-0.098
Random 10	0.156	0.024	-0.105
Random Models Parameters			
Average	0.116	0.022	-0.096

Interpretation of model CoMFA contour.

To provide us with clues about the change in chemical composition, a detailed study of the graphical contour maps was performed. Figure 3 shows the contour maps of the selected CoMFA/SE model. The green contours indicate regions favorable for large clustering to increase the activity of the molecule, while the yellow contours indicate regions unfavorable for large clustering to increase the activity (Figure 3A). A medium-sized green contour surrounds a region close to the variant R, indicating that the addition of a large cluster favors better activity. It explained by the

fact that compound 9 ($pIC_{50} = 6.36$), which contains a $-CH_3$ radical in R, has higher activity than compound 8 ($pIC_{50} = 5.17$), which contains a hydrogen H in the same radical, and the same is true for compounds 21 ($pIC_{50} = 7.81$) and 20 ($pIC_{50} = 6.47$). The blue and red color curves, respectively, show the areas where electropositive and electronegative groups are beneficial for activity (Figure 3B). A small red spot near the R1 substituent in the para position of the molecule shows that adding attractive mesomeric groups or strongly electronegative atoms at this location makes inhibition stronger.

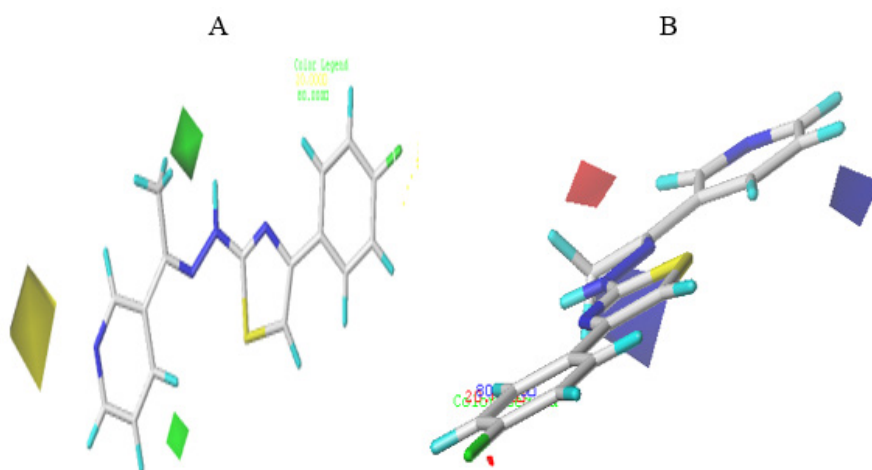


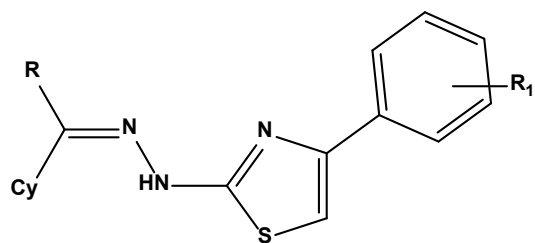
Figure 3. Contour map results of the best developed CoMFA/SE model: (A) Steric field and (B) electrostatic field.

Newly designed compounds

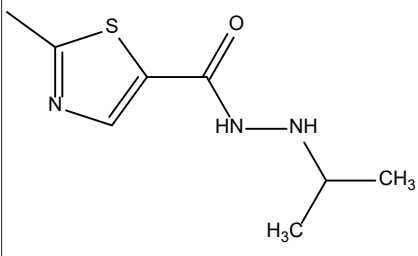
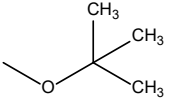
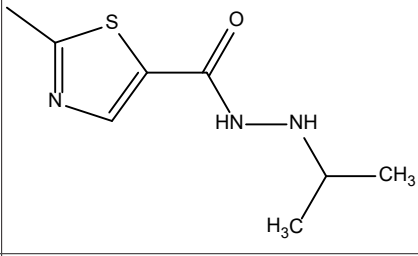
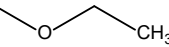
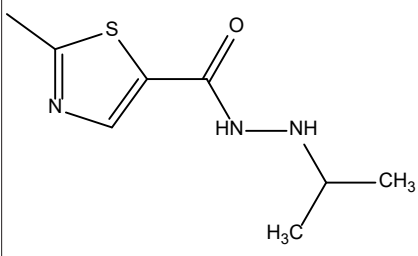
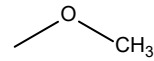
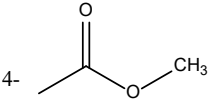
The initial factors affecting the inhibitory activity were identified based on the chemical structures of the proposed (4-*alt*-thiazole-2-yl) hydrazine derivatives,

where the substitutes fitted in appropriate positions utilizing contour maps by using the best CoMFA/SE model that predicts the activity of newly designed candidates, and the data tabulated in (Table 7).

Table 7. Anticipate new designs with their activities and docking score with the CoMFA/SE model.



No	Structure			Predicted pIC ₅₀	Total Score
	Cy	R	R1	CoMFA (SE)	
Comp26		CH ₃	4-F	8.458	10.5
M1			4-	10.4	11.6
M2			4-	9.73	11.2
M3			4-	9.72	10.2

M4			4-F	9.5	09.7
M5			4-F	9.024	10.8
M6			4- 	8.087	11.3

ADME-Tox prediction Drug similarity analysis

The prediction of ADMET characteristics is an essential step to reduce potential subsequent problems in clinical therapies. Therefore, pkCSM (Balerna, Fosset, Chicheportiche, Romey and Lazdunski, 1975) and SwissADME (Parr, Mulley and Rye, 1979) were adopted to predict the ADMET properties of the new (hetero)arylidene-(4-substituted-thiazol-2-yl)hydrazines. (Table 8) shows the Lipinski property profile of the proposed new molecules, while (Table 9) reveals the *in silico* ADMET properties of the new compounds M1, M2, M3, M4, M5, M6, and 26. For a given compound with logP less than 5, molecular weight (MW) (≤ 500 Da), hydrogen bond acceptors (HBAs) less than 10, and hydrogen bond donors (HBDs) less than 5, are considered the best-adsorbed drugs (Base the Lipinski Five). (Table 8) shows that molecules M1, M2, M3, M4, M5, M6, and 26 have logP less than 5, MW less than 500 Da, HBA less than 10 and HBD less than 5, In addition, the total polar area (TPSA) is less than 140 μM , and

the ring bonds (NROTb) are less than 10, indicating that these compounds have better adsorption and bioavailability (Jain, Guin, De and Singh, 2022).

A compound with an intestinal absorption value greater than 30% is also considered resorbable. As shown in (Table 9), all compounds have a value between 50.56% and 92.30%, indicating a good level of intestinal absorption. Cytochrome P450 is an essential enzyme system for drug metabolism in the liver. CYP3A4 is a major variant of cytochrome P450. All proposed molecules are inhibitors and substrates of CYP3A4. In addition, it is important to know the toxicity of the compounds, as an effective drug does not have to be toxic. To this end, the toxicity of the compounds was examined using the Ames test. The results showed that all the newly designed particles were non-toxic, except for the reference compound 26, which remains toxic. For all predicted compounds, the synthetic accessibility score was between 2.95 and 4.36, indicating that they are easily synthesized.

Table 8. Lipinski properties of the new M1-M6 compounds and the reference compound 26.

	26	M1	M2	M3	M4	M5	M6
Lipinski	YES	YES	YES	YES	YES	YES	YES
Log kp (cm/s)	-5.49	-6.09	-5.94	-4.10	-5.25	-5.51	-6.11
Log S	-4.49	-5.04	-5.25	-7.48	-6.02	-5.51	-6.11
Log P	4.18	3.35	3.43	3.8	4.63	3.85	3.11
nHBD	1	4	3	4	3	3	3
nHBA	4	8	8	8	7	8	8
TPSA	78.41	185.08	174.08	194.31	157.01	157.01	183.31
Nrotb	4	9	10	11	9	9	11
MR	87.59	113.12	117.44	128.58	126.42	116.77	123.28
MW	312.36	448.49	462.52	488.58	476.60	448.549	340.42

Table 9. In silico ADMET properties of the proposed new compounds and reference compound 26.

Comp	Intestinal absorption (human) Numeric (% Absorbed)	CYP1A2 inhibitor	CYP2C19 inhibitor	CYP2C9 inhibitor	CYP2D6 inhibitor	CYP3A4 inhibitor	AMES toxicity	Synthetic Accessibility
26	92.304	YES	YES	YES	NO	YES	YES	2.95
M1	85.11	YES	NO	YES	NO	YES	NO	3.89
M2	78.66	YES	NO	YES	NO	YES	NO	4.03
M3	50.56	NO	NO	NO	NO	YES	NO	4.32
M4	83.12	NO	YES	YES	NO	YES	NO	4.36
M5	88.18	YES	NO	YES	NO	YES	NO	4.13
M6	68.50	NO	NO	YES	NO	YES	NO	4.17

Docking results

To understand the quantitative link between structure and activity provided by the 3D-QSAR model, it is necessary to understand the method of ligand-receptor binding, which is typically studied by molecular docking. Using the online web service Atlas of Protein Communications, we identified the amino acids of interest, evaluated their chemical characteristics, and examined the important residues in the active site prior to docking (<http://www.mrc-lmb.cam.ac.uk/pca/>). The asteroid diagram, a new method of interaction analysis, uses a multilayer

representation of non-covalent interactions. The Protein Contact Atlas was used to create asteroid diagrams of these protein structures (Figure 4A) (El Bahi, Boutalaka, Alaqarbeh, et al., 2023). For amino acids that form strong contacts with the first shell amino acids, Arg42, Glu34, Glu58, Met436, Tyr398, Tyr435, Tyr60, and Arg41, all have significant affinity for hMAO-B. The number of atomic connections is also indicated by the thickness of the blue matrices in (Figure 4B). These results provided us with the crucial data we needed to evaluate the response patterns of the chemicals studied.

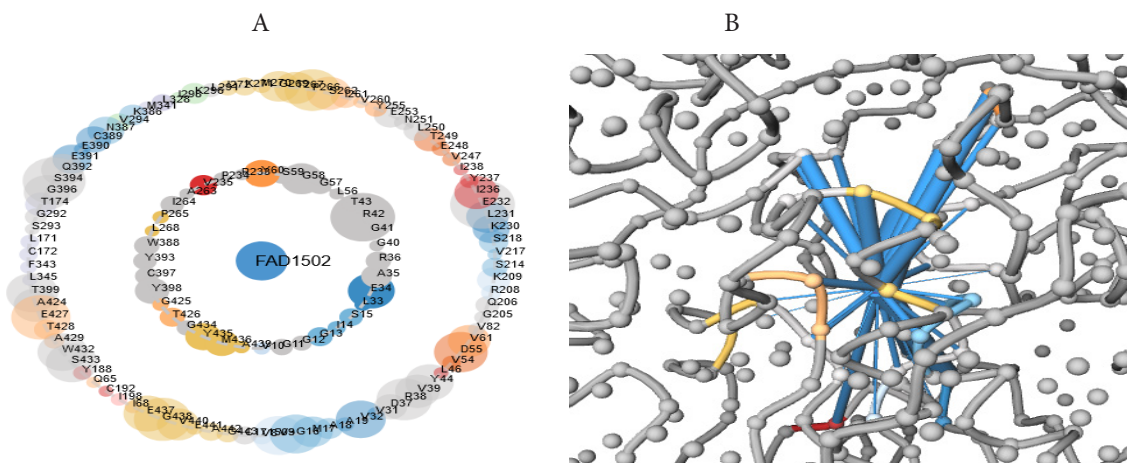


Figure 4. Asteroid graph and network view of protein-ligand interactions.

In order to validate the 3D QSAR method, this section focuses on the molecular docking methodology to obtain data on the structural basis and likely interaction between the ligand variants and the receptor. (Figure 4 and 5) illustrate the molecular docking interactions between the most active molecule 26, the recommended compound M1, and the hMAO-B receptor (PDB: 2V60). As shown in (Figure 5), compound 26 exhibits conventional hydrogen bonding interactions with residues Ile14, Ser15, and Gly434. A stacked Pi-pi interaction with residues Tyr398, Tyr435. a Pi-sulfur interaction with residue Cys397. Pi-alkyl interactions with residues Ala439, Arg42, Met436, Tyr398. and a Pi-sigma interaction with residue Tyr435. The presence of these interactions increases their biochemical efficiency as hMAO-B inhibitors. Using CB-DOCK software, the docking score was -10.5 kcal/mol. The interactions of the complex (compound M1- hMAO-B) were presented as shown in (Figure 6), which shows a Pi-pi interaction stacked with residue Tyr435. a Pi-alkyl interaction with residues Ala439, Arg42, and Met436,

In addition(Moulay Ahfid El Alaouy et al., 2021). a Pi-sulfur interaction with residues Cys397 and Tyr60. a hydrogen-carbon bond interaction with residue Gly13 and Glu58. And a stacked Pi-amide interaction with residue Tyr435. Similarly, for hydrogen bonding, classical hydrogen bonding type interactions are observed with residues Ile14, Ser15, Gln206, Met436, Tyr435, Tyr60, and Ser59. This binding plays a major role in the stability of the molecules. Due to the higher contacts of compound M1 with hMAO-B enzyme residues, the docking score was -11 kcal/mol, which is better than that of compound 26. The key residues obtained in the docking results presented above corresponded to the critical residues in the large circles of the AChE main chain. The type and number of interactions indicate that the M1 molecule has strong inhibitory activity against the hMAO-B enzyme. In addition, the results showed that the recommended chemical compound M1 has higher stability for the active site of hMAO-B enzyme. At the same time, the 3D-QSAR and docking results were consistent.

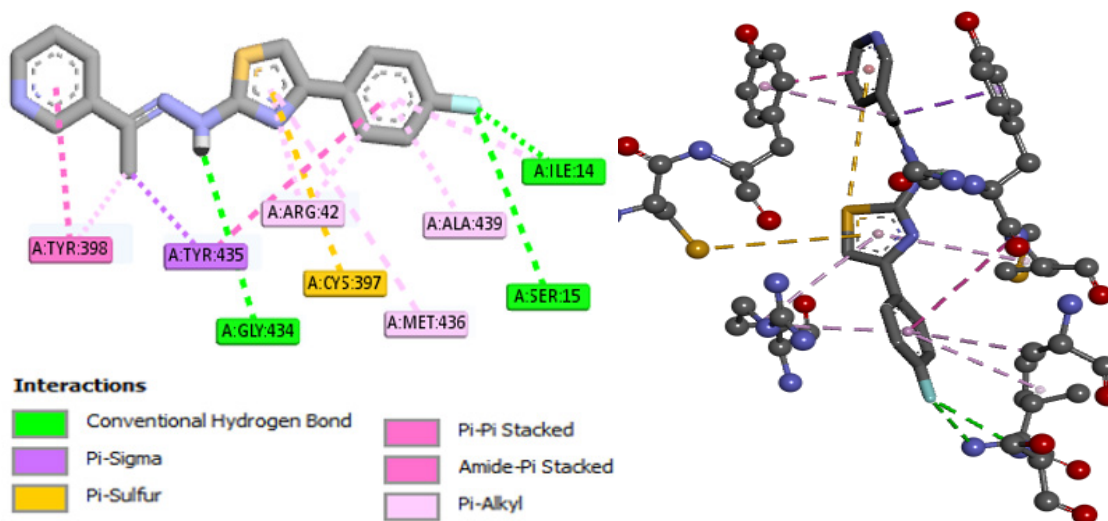


Figure 5. 2D and 3D Docking represent the interactions of the most active compounds at receptor binding sites.

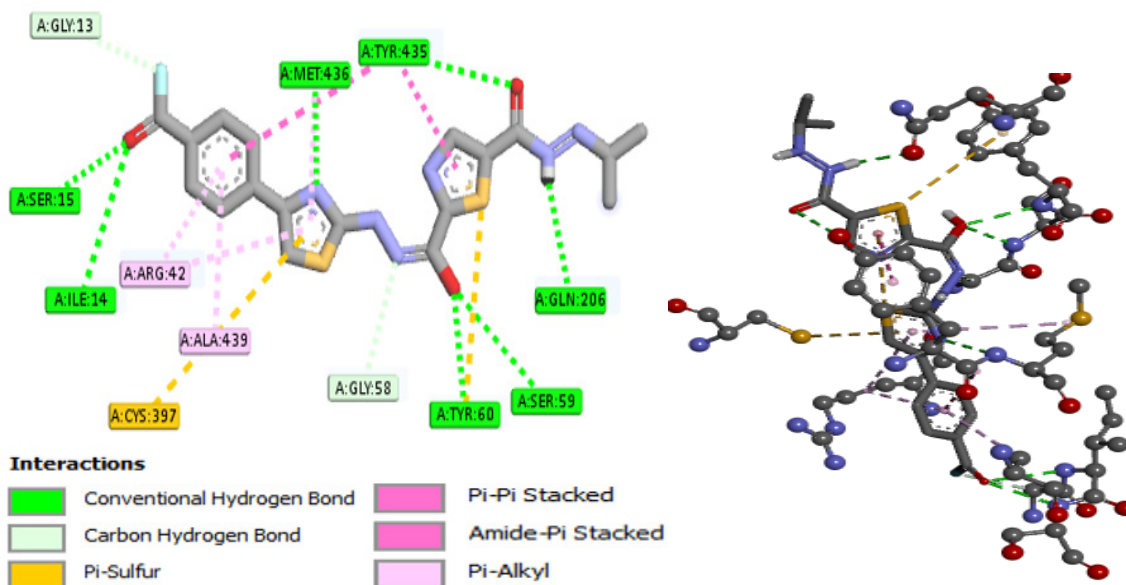


Figure 6. 2D and 3D Docking represent the interactions of the most active compound M1 at receptor binding sites.

Stability of protein-bond interactions in MD simulations

The binding stability of the two best compounds, hMAO-B-26 and hMAO-B-M1, was investigated using simulated MD calculations for 100 ns at typical room temperature settings. After simulation, visualization of the tracks indicated that all ligands remained bound to the protein pocket via the ligand-binding groove. To test the stability of each structure, RMSD, RMSF, 556

radius of rotation, hydrogen bonding, mean center of mass (COM) between protein and linker, and binding free energy calculations (MMPBSA) were performed to assess the stability of each structure (El Alaouy et al., 2023).

RMSD graphs in (Figure 7A) show the complex, protein backbone and ligand RMSD for each structure. Complex and Backbone RMSD show an increasing and fluctuating pattern for both complexes until it

stabilizes at 70ns for Comp26 and 50ns for M1 with average values of 3.8Å and 4Å, respectively. The radius of gyration analysis (Figure 7C) is also consistent with RMSD results for the complexes, showing very little fluctuations for both compounds (less than 1 Å) with values between 23.5 and 24. Å for Comp26 and 23.3 and 23.9 Å for M1 throughout the whole simulation, which indicates the compactness and the stability of the protein-ligand system (El Alaouy et al., 2023).

Using the GROMACS software, the RMSF of the protein complex was determined based on the “C-alpha” atoms. In general, the fluctuation intensity remains below 2.0 for all compounds, except for a few residues that are loops or spins in the protein (Figure 7B).

(Figure 8A), shows the total number of hydrogen bonds created between the ligand and the protein during the 100 ns of the simulation. Both ligands maintained at least one hydrogen bond with the protein during the whole simulation time. (Figure 8B) shows the average distance of the center of mass between the ligand and the protein during 100 ns of simulation time. Both ligands maintain a stable COM distance from the protein within 2 Å or less of fluctuations. Using the contact Freq.tcl module in VMD and a threshold of 4 Å, a contact frequency (CF) study was performed to better assess the binding between the [protein] and the ligands tested. The residues with higher CF% are shown in (Figure 9). The residues with the highest contact frequency in all simulations were ILE14, ARG42, GLY58, TYR60, LEU171, CYS172, PHE343, TYR398, THR4,

GLY434, TYR435, MET436 and ALA439. Principal Component Analysis (PCA) of the complexes was performed using the Bio3D program in R, and the results are depicted in (Figure 10 A). Additionally, the program was used to calculate the dynamic cross-correlated motions (DCCM) of protein residues. The DCCM analysis assigns colors ranging from red to white to blue, indicating the intensity of correlated motion between residues. Blue colors represent negative correlation, white indicates no correlation, and red color signifies positive correlation in the motions between residues. (Figure 10 B).

MM/PBSA (Molecular Mechanics/Poisson Boltzmann Surface Area) method is a fast force field-based approach for calculating bond free energies. The G-mmpbsa software was utilized in this study to compute the MM/PBSA values. The calculated binding free energy values are presented in (Table 10). In conclusion, compounds M1 and 26 exhibited remarkable stability throughout the 100 ns MD simulation based on analyses of RMSD, Rg, RMSF, SASA, and hydrogen bonding between the protein and ligand. Additionally, the average distance between the ligand and protein complexes remained consistent. However, pathway analysis and MM/PBSA measurements of binding free energy revealed that compound 26 exhibited the highest binding free energy, while compound M1 exhibited the lowest binding free energy. Therefore, compound M1 demonstrated higher activity as an enzyme inhibitor compared to compound 26.

Table 10. Calculated binding free energies of tested compounds [kJ/mol]

Complex	ΔG	Van der Waal Energy	Electrostatic energy	Polar solvation energy	SASA energy
Comp26	- 134.288 +/- 15.082 kJ/mol	-199.514 +/- 8.970 kJ/mol	-94.064 +/- 14.525 kJ/mol	178.053 +/- 10.415 kJ/mol	-18.764 +/- 0.576 kJ/mol
M1	-150.506 +/- 12.354 kJ/mol	281.052 +/- 7.595 kJ/mol	63.585 +/- 12.016 kJ/mol	219.398 +/- 14.268 kJ/mol	-25.267 +/- 0.887 kJ/mol

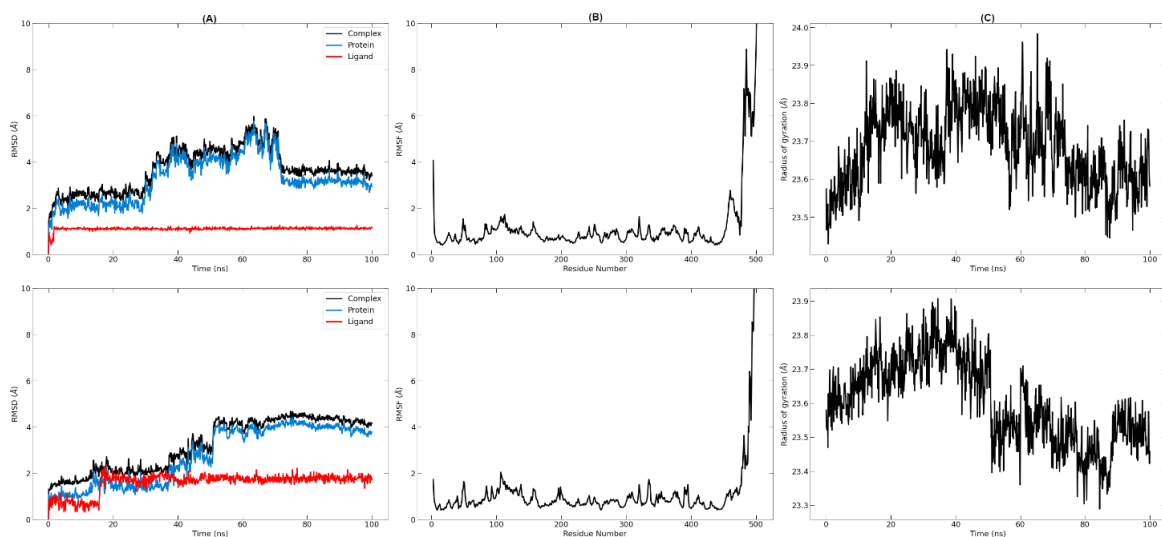


Figure 7. (A) RMSD, (B) RMSF and (C) Radius of gyration of the complexes during 100ns MD simulation. Compounds Comp26 (top) and M1 (bottom)

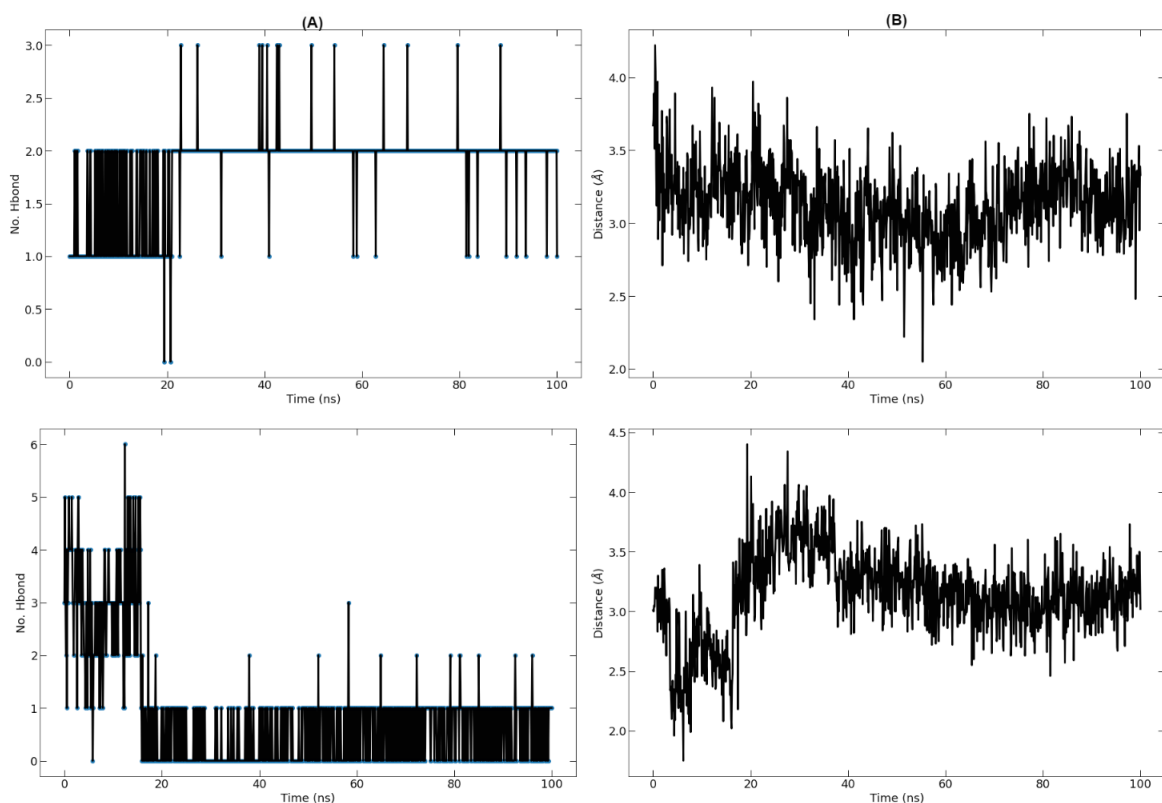


Figure 8. (A) Hydrogen Bonds (Protein-ligand) and (B) Average distance between Ligand and the Protein of the complexes during 100ns MD simulation. Compounds Comp26 (top) and M1 (bottom)

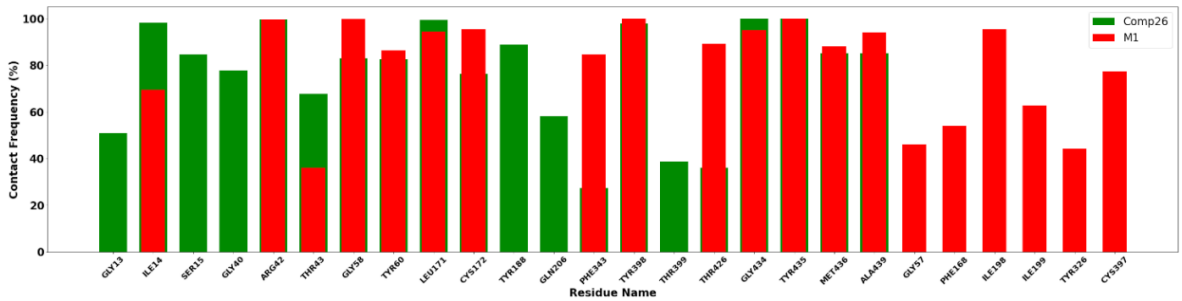


Figure 9. Contact frequency analysis

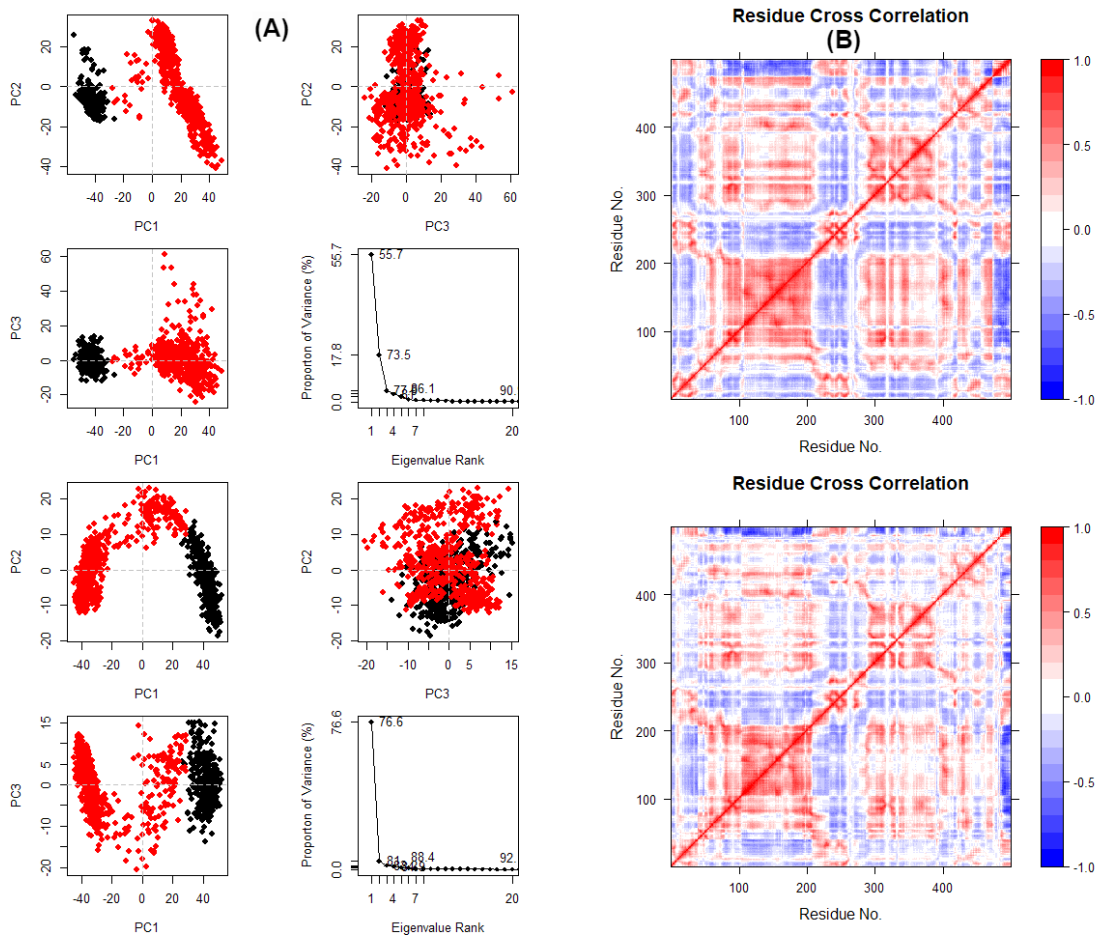


Figure 10. From left to right: (A) Principal Component Analysis and (B) Dynamic Cross-Correlation Matrix Analysis (DCCM).

CONCLUSION

Monoamine oxidase B (hMAO-B) is an attractive target for drug design because its inhibition regulates the levels of various neurotransmitters in the central nervous system. Molecules that act selectively on one of the hMAO-B isoforms have been widely studied. In this manuscript, 3D-QSAR models were developed using CoMFA/SE, and the excellent statistical results ($Q^2 = 0.608$; $R^2 = 0.933$; $R^2_{Test} = 0.7$) indicate that the CoMFA/SE model has excellent predictive capabilities. Furthermore, the contour maps generated by the best CoMFA/SE model were used to develop new derivatives with increased activity. Furthermore, the docking simulations were confirmed by highlighting the potential interactions of the proposed compound M1 and the reference compound 26 with the crystal structure of hMAO-B. Molecular docking between the proposed M1 complex and the protein crystal structure (PDB: 2V60) showed that it underwent a classical hydrogen-bonding type interaction with the major and non-key residues Ile14, Ser15, Gln206, Met436, Tyr435, Tyr60, and Ser59 as well as other interactions more important than complex 26, where hydrogen bonds are responsible for the inhibitory activity (Hirenallure Maheshwarappa et al., 2022). Thus, the proposed M2 complex is more stable towards the selected protein than the reference complex 26. In addition, the MD simulation results show that both studied compounds are well stable based on the analyses of (RMSD, RMSE, RG, Contact frequency analysis, hydrogen bonding (protein-ligand) and the average distance between the bond and the protein complexes during 100 ns. Furthermore, compound 26 and the proposed compound M1 showed hMAO-B binding free energies of -134.288 kJ/mol and -150.506 kJ/mol, respectively. Thus, it can be said that compound M1 is more active than compound 26. For these newly designed molecules, prediction of Lipinski's rule and ADMET properties is essential, and similarities were observed in their pharmacokinetics. The compounds generally have good absorption, distribution and metabolism

properties and are non-toxic, except for the reference compound 26 which remains toxic. The results obtained in this work clearly indicate that compound M1 has a strong potential to become promising in the treatment of several neurodegenerative diseases, such as Parkinson's diseases.

AUTHOR CONTRIBUTION STATEMENT

Moulay Ahfid El Alaouy: article writing, graph preparation, data analysis and interpretation; Marwa Alaqarbeh: paper writing, analyzed and interpreted molecular dynamic simulation data; Abdelouahid Sbai, Tahar Lakhlifi and Mohammed Bouachrine: project review, editing and supervision.

CONFLICT OF INTEREST

The authors declare that there is no conflict of interest.

REFERENCES

- Aanouz, I., Belhassan, A., El-Khatibi, K., Lakhlifi, T., El-Idrissi, M. and Bouachrine, M. (2021). Moroccan Medicinal plants as inhibitors against SARS-CoV-2 main protease: Computational investigations. *Journal of Biomolecular Structure and Dynamics*, 39(8), 2971-2979. doi:10.1080/07391102.2020.1758790
- Anastassova, N., Aluani, D., Hristova-Avakumova, N., Tzankova, V., Kondeva-Burdina, M., Rangelov, M., ... Yancheva, D. (2022). Study on the Neuroprotective, Radical-Scavenging and MAO-B Inhibiting Properties of New Benzimidazole Arylhydrazones as Potential Multi-Target Drugs for the Treatment of Parkinson's Disease. *Antioxidants*, 11(5), 884. doi:10.3390/antiox11050884
- Balerna, M., Fosset, M., Chicheportiche, R., Romey, G. and Lazdunski, M. (1975). Constitution and properties of axonal membranes of crustacean nerves. *Biochemistry*, 14(25), 5500-5511. doi:10.1021/bi00696a019

- Boutalaka, M., El Bahi, S., Alaqrbeh, M., El Alaouy, M. A., Koubi, Y., Khatabi, K. E., ... Lakhlifi, T. (2023). Computational investigation of imidazo[2,1-b]oxazole derivatives as potential mutant BRAF kinase inhibitors: 3D-QSAR, molecular docking, molecular dynamics simulation, and ADMETox studies. *Journal of Biomolecular Structure and Dynamics*, 1-20. doi:10.1080/07391102.2023.2233629
- Bozbey, İ., Taşkor Önel, G., Türkmenoğlu, B., Gürsoy, Ş. and Dilek, E. (2022). Novel (p-tolyl)-3(2H)-pyridazinone derivatives containing substituted-1,2,3-triazole moiety as new anti-Alzheimer agents: Synthesis, in vitro and in silico assays. *Fabad Journal of Pharmaceutical Sciences*. doi:10.55262/fabadeczacilik.1128446
- Cao, Y. and Li, L. (2014). Improved protein–ligand binding affinity prediction by using a curvature-dependent surface-area model. *Bioinformatics*, 30(12), 1674-1680. doi:10.1093/bioinformatics/btu104
- Chimenti, F., Maccioni, E., Secci, D., Bolasco, A., Chimenti, P., Granese, A., ... Distinto, S. (2007). Selective Inhibitory Activity against MAO and Molecular Modeling Studies of 2-Thiazolylhydrazone Derivatives. *Journal of Medicinal Chemistry*, 50(4), 707-712. doi:10.1021/jm060869d
- Chimenti, F., Secci, D., Bolasco, A., Chimenti, P., Granese, A., Carradori, S., ... Langer, T. (2010). Synthesis, semipreparative HPLC separation, biological evaluation, and 3D-QSAR of hydrazothiazole derivatives as human monoamine oxidase B inhibitors. *Bioorganic & Medicinal Chemistry*, 18(14), 5063-5070. doi:10.1016/j.bmc.2010.05.070
- Daina, A., Michielin, O. and Zoete, V. (2017). SwissADME: A free web tool to evaluate pharmacokinetics, drug-likeness and medicinal chemistry friendliness of small molecules. *Scientific Reports*, 7(1), 42717. doi:10.1038/srep42717
- Dhiman, P., Malik, N., Sobarzo-Sánchez, E., Uriarte, E. and Khatkar, A. (2019). Quercetin and Related Chromenone Derivatives as Monoamine Oxidase Inhibitors: Targeting Neurological and Mental Disorders. *Molecules*, 24(3), 418. doi:10.3390/molecules24030418
- El Alaouy, M. A., El Bahi, S., Boutalaka, M., Ouabane, M., Sbai, A., Maghat, H., ... Lakhlifi, T. (2023). Organic compounds based on 1-(prop-2-yn-1-ylamino)-2,3-dihydro-1H-indene-4-thiol as selective human monoamine oxidase B inhibitors. Quantitative analysis of structure-activity relationships and in-silico investigations. *Moroccan Journal of Chemistry, Vol. 11, Mor. J. Chem. 11 N°3 (2023) 802-817 Pages*. doi:10.48317/IMIST.PRSM/MORJCHEM-V11I3.40986
- El Alaouy, Moulay Ahfid, Alaqrbeh, M., Ouabane, M., Zaki, H., ElBouhi, M., Badaoui, H., ... Bouachrine, M. (2023). Computational Prediction of 3,5-Diaryl-1H-Pyrazole and spiropyrazolines derivatives as potential acetylcholinesterase inhibitors for alzheimer disease treatment by 3D-QSAR, molecular docking, molecular dynamics simulation, and ADME-Tox. *Journal of Biomolecular Structure and Dynamics*, 1-14. doi:10.1080/07391102.2023.2252116

- El Alaouy, Moulay Ahfid, Youness, M., Boutalaka, M., Elbouhi, M., Elmernissi, R., Sbai, A., ... Bouachrine, M. (2021). The 2D-QSAR study, Drug likeness and in-silico ADMET prediction of about 3,5-diaryl-1H-pyrazole derivatives as multifunctional agents for the treatment of Alzheimer's disease. *RHAZES: Green and Applied Chemistry*, 09-28 Pages. doi:10.48419/IMIST.PRSM/RHAZES-V13.28095
- El Bahi, S., Boutalaka, M., Alaqarbeh, M., El Alaouy, M. A., Koubi, Y., El Khatabi, K., ... Lakhlifi, T. (2023). In-Silico Investigation of Osimertinib Based Compounds as Potential Double Mutant EGFR Kinase Inhibitors Against H1975 Cell Line: Integrating QSAR Modeling, Molecular Docking, MD Simulations, and ADME/Tox Studies. *Chemistry Africa*. doi:10.1007/s42250-023-00744-x
- El Bahi, S., Boutalaka, M., El Alaouy, M. A., Bouamrane, S., Alaqarbeh, M., Choukrad, M., ... Lakhlifi, T. (2023). Computational investigation of novel pyrimidine derivatives as potent FAK inhibitors via 3D-QSAR, molecular docking, molecular dynamics simulation and retrosynthesis. *New Journal of Chemistry*, 47(27), 12816-12829. doi:10.1039/D3NJ02471G
- Fiddian-Green, R. and Silen, W. (1975). Mechanisms of disposal of acid and alkali in rabbit duodenum. *American Journal of Physiology-Legacy Content*, 229(6), 1641-1648. doi:10.1152/ajplegacy.1975.229.6.1641
- Hirenallure Maheshwarappa, C., Kamsagara Linganna, K., Bommenahalli Revanappa, P. K., Mehdi, S., Ayachit, S., Suman, S., ... Eswaran, S. (2022). Novel Glitazones Reverses Hyperglycemia In STZ Induced Hyperglycaemic Rat Model. *Fabad Journal of Pharmaceutical Sciences*, 73-82. doi:10.55262/fabadeczacilik.1078895
- Jain, P., Guin, M., De, A. and Singh, M. (2022). Molecular docking, synthesis, anticancer activity, and computational investigations of thiazole-based ligands and their Cu(II) complexes. *Journal of Physical Organic Chemistry*, e4384. doi:10.1002/poc.4384
- Kahn, T., Bosch, J., Levitt, M. F. and Goldstein, M. H. (1975). Effect of sodium nitrate loading on electrolyte transport by the renal tubule. *The American Journal of Physiology*, 229(3), 746-753. doi:10.1152/ajplegacy.1975.229.3.746
- Kidder, G. W. and Montgomery, C. W. (1975). Oxygenation of frog gastric mucosa in vitro. *The American Journal of Physiology*, 229(6), 1510-1513. doi:10.1152/ajplegacy.1975.229.6.1510
- Kondeva-Burdina, M., Mitkov, J., Valkova, I., Peikova, L., Georgieva, M. and Zlatkov, A. (2022). Quantitative Structure-Neurotoxicity Assessment and In Vitro Evaluation of Neuroprotective and MAO-B Inhibitory Activities of Series N-substituted 3-(1,3,7-trimethylxanthin-8-ylthio)propanehydrazides. *Molecules*, 27(16), 5321. doi:10.3390/molecules27165321
- Lévêque-Simon, K., Camper, A., Taïeb, R., Caillat, J., Lévêque, C. and Giner, E. (2023). Production of positronium chloride: A study of the charge exchange reaction between Ps and Cl. doi:10.48550/ARXIV.2305.17078
- Lipscomb, T. P., Scott, D. P. and Schulman, F. Y. (2010). Primary site of sea lion carcinomas. *Veterinary Pathology*, 47(1), 185; author reply 186. doi:10.1177/0300985809354348

- Liu, Y., Grimm, M., Dai, W., Hou, M., Xiao, Z.-X. and Cao, Y. (2020). CB-Dock: A web server for cavity detection-guided protein–ligand blind docking. *Acta Pharmacologica Sinica*, 41(1), 138-144. doi:10.1038/s41401-019-0228-6
- Lu, Y., Gao, X., Dong, Y., Wang, T., Chen, H.-L., Maob, H., ... Guo, S. (2018). Preparing bulk ultrafine-microstructure high-entropy alloys via direct solidification. *Nanoscale*, 10(4), 1912-1919. doi:10.1039/C7NR07281C
- Nagatsu, T. (1997). Isoquinoline neurotoxins in the brain and Parkinson's disease. *Neuroscience Research*, 29(2), 99-111. doi:10.1016/S0168-0102(97)00083-7
- Pajzderska, A. and Gonzalez, M. A. (2023). Molecular Dynamics Simulations of Selected Amorphous Stilbenoids and Their Amorphous Solid Dispersions with Poly(Vinylpyrrolidone). *Journal of Pharmaceutical Sciences*, 112(9), 2444-2452. doi:10.1016/j.xphs.2023.03.013
- Parr, G. D., Mulley, B. A. and Rye, R. M. (1979). The effect of carbonic anhydrase binding on the pharmacokinetics of chlorthalidone [proceedings]. *The Journal of Pharmacy and Pharmacology*, 31 Suppl, 42P. doi:10.1111/j.2042-7158.1979.tb11590.x
- Pires, D. E. V., Blundell, T. L. and Ascher, D. B. (2015). pkCSM: Predicting Small-Molecule Pharmacokinetic and Toxicity Properties Using Graph-Based Signatures. *Journal of Medicinal Chemistry*, 58(9), 4066-4072. doi:10.1021/acs.jmedchem.5b00104
- Secci, D., Bolasco, A., Carradori, S., D'Ascenzio, M., Nescatelli, R. and Yáñez, M. (2012). Recent advances in the development of selective human MAO-B inhibitors: (Hetero)arylidene-(4-substituted-thiazol-2-yl)hydrazines. *European Journal of Medicinal Chemistry*, 58, 405-417. doi:10.1016/j.ejmech.2012.10.032
- Shaukat, A. and Hussain, K. (2022). Quercetin Based Standardization Of Polyherbal Anti-Gout Remedy And Its Molecular Docking Study Against Anti-Gout And Anti-Inflammatory Protein Targets. *Fabad Journal of Pharmaceutical Sciences*. doi:10.55262/fabadeczacilik.1085825
- Stamm, O., Latscha, U., Janecek, P. and Campana, A. (1976). Development of a special electrode for continuous subcutaneous pH measurement in the infant scalp. *American Journal of Obstetrics and Gynecology*, 124(2), 193-195. doi:10.1016/s0002-9378(16)33297-5
- Şener, K., Ekici, M., Gönülalan, E. M. and Bodur, E. (2024). Comparative Study of The Anti-Inflammatory Pathway Enzyme Activities of Selected Plant Extracts from Lamiaceae Family. *Fabad Journal of Pharmaceutical Sciences*. doi:10.55262/fabadeczacilik.1391109
- Vicente-Zurdo, D., Brunetti, L., Piemontese, L., Guedes, B., Cardoso, S. M., Chavarria, D., ... Santos, M. A. (2023). Rivastigmine–Benzimidazole Hybrids as Promising Multitarget Metal-Modulating Compounds for Potential Treatment of Neurodegenerative Diseases. *International Journal of Molecular Sciences*, 24(9), 8312. doi:10.3390/ijms24098312

- Yang, C., Wang, W., Liang, J.-X., Li, G., Vellaisamy, K., Wong, C.-Y., ... Leung, C.-H. (2017). A Rhodium(III)-Based Inhibitor of Lysine-Specific Histone Demethylase 1 as an Epigenetic Modulator in Prostate Cancer Cells. *Journal of Medicinal Chemistry*, 60(6), 2597-2603. doi:10.1021/acs.jmedchem.7b00133
- Yücel, Y. Y. and Özdemir, E. (2023). Determination of Biological Activities of *Salvia sclarea* L. *Fabad Journal of Pharmaceutical Sciences*. doi:10.55262/fabadeczacilik.1293118
- Zwahlen, T. A. (2023). Landscapes of DNA Mechanics and Genomes. doi:10.5075/EPFL-THESIS-8784